Modeling and Simulation of a Powered Exoskeleton System to Aid Human-Robot Collaborative Lifting

Asif Arefeen and Yujiang Xiang*
School of Mechanical and Aerospace Engineering
Oklahoma State University, Stillwater, OK 74078, USA
*Corresponding Author: yujiang.xiang@okstate.edu

Abstract

Exoskeletons are remarkable technologies that improve human strength, reduce fatigue, and restore users' abilities. In this study, a novel physics-based optimization formulation is proposed to find the optimal control of a powered elbow exoskeleton to aid the human-robot collaborative lifting task. The three-dimensional (3D) human arm model has 13 degrees of freedom (DOFs), and the 3D robot arm (Sawyer robot arm) model has 10 DOFs. The inverse dynamics optimization is utilized to find the optimal lifting motion and the optimal exoskeleton assistive torque. The 3D human arm and robot arm are modeled in Denavit-Hartenberg (DH) representation. The electromechanical dynamics of the DC motor of the exoskeleton are considered in the dynamic human-robot collaborative lifting optimization. In addition, the 3D box is modeled as a floating-base rigid body with 6 global DOFs. The human-box and robot-box interactions are characterized as a collection of grasping forces. The joint torque squares of human arm and robot arm are minimized subjected to physics- and task-based constraints. The design variables include (1) control points of cubic B-splines of joint angle profiles of the human arm, robotic arm, and box; (2) control points of cubic B-splines of motor current for the exoskeleton; and (3) the discretized grasping forces during lifting. The constraints include joint angle limits for human arm and robot arm, joint torque limits for human arm, robot arm and exoskeleton, human-robot grasping positions, box balance condition, initial and final box locations, and bounds on design variables. A numerical example of lifting a 10 kg box is simulated. The nonlinear collaborative lifting optimization problem is solved using a sequential quadratic programming (SQP) method in SNOPT, and the optimal solutions are found in 136.11 seconds. The simulation reports the grasping force profiles, human arm's joint angles, and the powered elbow exoskeleton's torque profiles. The results reveal that the proposed optimization formulation can find the exoskeleton's optimal control and lifting strategy for the human-robot collaborative lifting task.

Keywords: Motion planning, optimal control, human-robot interaction, powered exoskeleton, and inverse dynamics optimization.

Introduction

Collaboration between humans and robots is a research topic with a wide range of applications and a major economic impact. Human-robot collaboration can considerably speed up production processes, improve manufacturing efficiency, and reduce structural costs. On the other hand, wearable devices such as exoskeletons have a wide range of applications in clinical neurorehabilitation settings and industrial settings for construction and manufacturing. These wearable technologies can improve a person's strength, minimize workplace fatigue, and restore a person's limited range of motion caused by diseases. In addition, the exoskeleton can prevent human injuries and increase human endurance during human-robot collaborative tasks. Therefore, human-robot collaborative lifting motion prediction with a powered exoskeleton is a state-of-the-art technology that has not been studied yet. Moreover, designing and simulating an optimal powered exoskeleton system is necessary to assist human-robot object lifting tasks.

Last few years, several optimization-based modeling methods have been used to simulate exoskeleton-wearer interaction (Agarwal et al., 2013; Bai & Rasmussen, 2011; Zhou et al., 2015). There have been a few studies on developing robotic exoskeletons to assist humans in lifting tasks. During manual lifting, a semi-squat lifting model was used to determine the hip joint output torque and power for the active hip exoskeleton to aid lifting motion (Wei et al., 2020). In Manns et al., (2017), a 2-DOF passive back exoskeleton was developed to aid the lifting motion. The spring parameters of the exoskeleton were optimized using an SQP-based direct multiple shooting method. In Zhang & Huang (2018), a compact series-elastic actuated 4-DOF powered hip exoskeleton was designed to alleviate lumbar compression by reducing muscular activities around the lumbar spine for both symmetric and asymmetric liftings. Xiang and Arefeen (2020) developed a human-human collaborative lifting motion prediction considering human-box grasping forces. In addition, an optimization-based human-robot collaborative lifting motion prediction has been developed in previous research (Arefeen et al., 2022a, 2022b; Arefeen & Xiang, 2021).

This work extends our previous collaborative lifting prediction for the 3D and 2D skeleton models (Arefeen et al., 2022b; Arefeen & Xiang, 2021; Xiang & Arefeen, 2020) to human-robot collaborative lifting with an elbow exoskeleton. This study proposes a novel physics-based optimization formulation to find the optimal control of a powered elbow exoskeleton to aid the human-robot collaborative lifting task. An inverse dynamics optimization formulation was used to optimize the lifting motion and exoskeleton control. An SQP algorithm in SNOPT (Gill et al., 2005) is used to solve the human-robot lifting problem. The simulation reports the human grasping force profiles, the human arm’s joint angles, and the powered elbow exoskeleton’s torque profiles.

Methods

This section discusses the 3D human arm model augmented by an active elbow exoskeleton and robot arm model. In addition, the floating-based 3D rigid box model is also discussed.

Human-exoskeleton and robot arm model

This work considers a 3D human skeletal arm model equipped with an active 1-DOF elbow exoskeleton, a 10-DOF robot arm model, and a rigid box, as shown in Figure 1. The human skeletal arm model has 13 DOFs. The box has 6 global DOFs, including three translations and three rotations. The human elbow joint is augmented by an active 1-DOF exoskeleton. The robotic formulation of the DH method is used to construct the human arm, robot and the box models. In addition, there are two grasping forces ($\mathbf{f}_{c1}$ and $\mathbf{f}_{c2}$) acting on the two bottom edges of the box. In this study, the human anthropometric data are obtained using GEBOD™ software (Cheng et al., 1994). The DH parameters for the human arm, robot arm, and box model are available in the literature (Arefeen & Xiang, 2021).

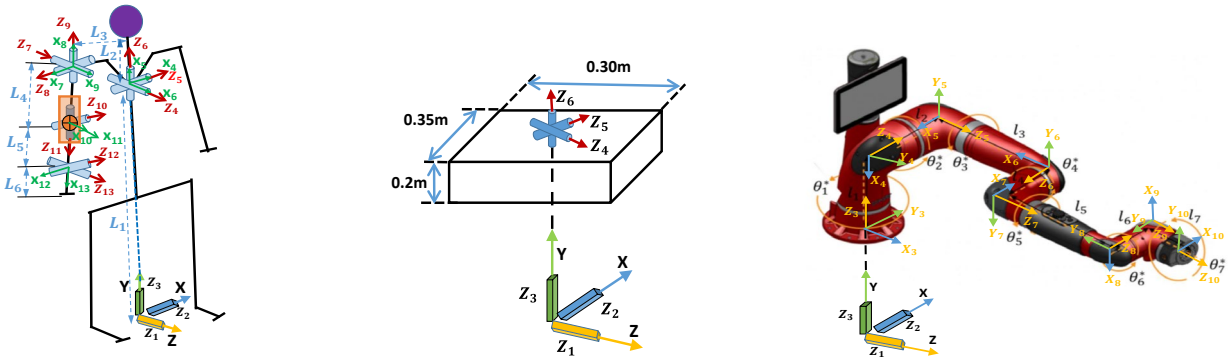

(a) (b) (c)

Figure 1. (a) The 3D human arm model (global DOFs: $z_1, z_2, z_3, z_4, z_5, z_6$) with an elbow exoskeleton (orange), (b) 3D box model (global DOFs: $z_1, z_2, z_3, z_4, z_5, z_6$), and (c) Sawyer robot arm (global DOFs: z_1, z_2, z_3).

Equation of motion (EOM)

The electromechanical dynamics of DC motors of the exoskeleton are modeled in the optimization-based dynamic human lifting motion prediction. The dynamics equations can be expressed as follow (Nguyen et al., 2020):

$$L\frac{dI}{dt} = V - K\frac{d\theta}{dt} - RI \tag{1}$$

$$T_{motor} = KI \tag{2}$$

$$T_l = T_{motor} - J_m \frac{d^2\theta}{dt^2} - b\frac{d\theta}{dt} \tag{3}$$

where V, I, L, and R are the voltage input, current, inductance, and resistance. The mechanical terms J_m, b, K, and θ are the rotor moment of inertia, coefficient of viscous friction of the motor, motor torque constant, and rotor angle. T_{motor} is the motor output torque and T_l is the load torque of the exoskeleton. The gearbox ratios (GB_r) are chosen so that the exoskeleton can provide the required torque output. Here, the exoskeleton includes the motor and the gearbox. So, the output torque (τ_e) of the exoskeleton can be expressed as follows:

$$\tau_e = GB_r \times T_l \tag{4}$$

The human-exoskeleton model is analyzed using recursive kinematics and Lagrangian dynamics (Xiang & Arefeen, 2020). Forward kinematics and backward dynamics are the two aspects of the process. The EOM of the human-exoskeleton systems and sensitivity analysis are formed using a recursive Lagrangian dynamics formulation. The dynamics can be expressed as follows:

$$\tau_{h_i} + \tau_{e_i} = \mathrm{tr}\left(\frac{\partial \mathbf{A}_i}{\partial q_i}\mathbf{D}_i\right) - \mathbf{g}^{\mathrm{T}}\frac{\partial \mathbf{A}_i}{\partial q_i}\mathbf{E}_i - \mathbf{f}_k^{\mathrm{T}}\frac{\partial \mathbf{A}_i}{\partial q_i}\mathbf{F}_i - \mathbf{G}_i^{\mathrm{T}}\mathbf{A}_{i-1}\mathbf{z}_0 \tag{5}$$

where τ_{h_i} is the actual human torque at the i^{th} joint and τ_{e_i} is the exoskeleton output torque for the i^{th} joint. $\mathbf{A}_i$ is the global position transformation matrices (4×4) for the i^{th} joint. $tr(\cdot)$ is the trace of a matrix $\mathbf{A}_i$, $\mathbf{C}_i$ are global position and acceleration transformation matrices, $\mathbf{I}_i$ is the inertia matrix for link i, $\mathbf{D}_i$ is the recursive inertia and Coriolis matrix, $\mathbf{E}_i$ is the recursive vector for gravity torque calculation, $\mathbf{F}_i$ is the recursive vector for external force-torque calculation, $\mathbf{G}_i$ is the recursive vector for external moment torque calculation, $\mathbf{g}$ is the gravity vector, m_i is the mass of link i, $\mathbf{r}_i$ is the COM of link i in the i^{th} local frame, $\mathbf{f}_k = [f_{kx} \quad f_{ky} \quad f_{kz} \quad 0]^{\mathrm{T}}$ is the external force applied on link k, $\mathbf{r}_k$ is the position of the external force in the k^{th} local frame, $\mathbf{h}_k = [h_x \quad h_y \quad h_z \quad 0]^{\mathrm{T}}$ is the external moment applied on link k, $\mathbf{z}_0 = [0 \quad 0 \quad 1 \quad 0]^{\mathrm{T}}$ is for a revolute joint, $\mathbf{z}_0 = [0 \quad 0 \quad 0 \quad 0]^{\mathrm{T}}$ is for a prismatic joint, finally, δ_{ik} is Kronecker delta, and the starting conditions are $\mathbf{D}_{n+1} = [\mathbf{0}]$ and $\mathbf{E}_{n+1} = \mathbf{F}_{n+1} = \mathbf{G}_{n+1} = [\mathbf{0}]$. The detailed formulas and sensitivity with respect to state variables are referred to Xiang & Arefeen (2020) and Xiang et al. (2009). Moreover, this study treats the grasping external forces of human-box and robot-box as unknowns (design variables) in the optimization formulation. As a result, the joint torques are a function of both state variables and varying grasping forces. To use gradient-based optimization, the sensitivity of joint

torque with respect to external force needs to be determined that was explained in detail in the literature (Arefeen et al., 2022a, 2022b).

Optimization formulation

The human-robot collaborative lifting is predicted by solving a nonlinear programming (NLP) problem. Here the box initial and final positions, the feet and robot base positions, and the box dimension and weight are given.

Design variables

The design variables (**x**) are cubic joint angle B-spline control points $\mathbf{P}_{human}$, $\mathbf{P}_{robot,}$ and $\mathbf{P}_{box}$ for the human, robot, and box. The motor current *I* profiles are also discretized using cubic B-splines so that the exoskeleton current control points $\mathbf{P}_{current}$ are also design variables. Furthermore, the grasping forces ($\mathbf{f}_1^c$ and $\mathbf{f}_2^c$) between human and box, and robot and box, are treated as additional design variables. As a result, the optimization design variables for the collaborative lifting are $\mathbf{x} = [\mathbf{P}_{human}^{\mathrm{T}} \quad \mathbf{P}_{robot}^{\mathrm{T}} \quad \mathbf{P}_{box}^{\mathrm{T}} \quad \mathbf{P}_{current}^{\mathrm{T}} \quad \mathbf{f}_{c1}^{\mathrm{T}} \quad \mathbf{f}_{c2}^{\mathrm{T}}]^{\mathrm{T}}$.

Objective function

The dynamics effort (Xiang & Arefeen, 2020) is used as the objective function for the collaborative lifting motion, which is defined as the sum of joint torques squared for human and robot (Arefeen & Xiang, 2020, 2021; Xiang & Arefeen, 2020; Xiang et al., 2009).

$$J(\mathbf{x}) = w_1 \sum_{i=6}^{n\_human} \int_0^T \{\tau_{i(human)}^2(\mathbf{P}_{human}, \mathbf{f}_1^c)\}dt + w_2 \sum_{i=3}^{n\_robot} \int_0^T \{\tau_{i(robot)}^2(\mathbf{P}_{robot}, \mathbf{f}_2^c)\}dt \quad (6)$$

where $n\_human = 13$, $n\_robot = 10$. The total time duration *T* is a specified input parameter, w_1 and w_2 are weighting coefficients for human and robot performance measure, respectively.

Constraints

The time-dependent constraints include joint angle limits, joint torque limits, human feet and robot base contacting position, box forward position, box range of motion, box grasping location, box global EOM, and exoskeleton torque limit. Time independent constraints include initial and final box locations, static conditions at the beginning and end of the motion. At each time discretization point, time-dependent constraints are sequentially determined during the optimization process. The time-independent constraints, however, are determined at a specific time point.

(a) Joint angle limits

$$\mathbf{q}_h^L \leq \mathbf{q}_h(\mathbf{x}, t) \leq \mathbf{q}_h^U \quad (7)$$
$$\mathbf{q}_r^L \leq \mathbf{q}_r(\mathbf{x}, t) \leq \mathbf{q}_r^U$$

where the superscript *L* and *U* denote the lower and upper bound of the limits, respectively. $\mathbf{q}_h$ and $\mathbf{q}_r$ are the joint angles for the human and robot arm.

(b) Joint torque limits

$$\boldsymbol{\tau}_h^L \leq \boldsymbol{\tau}_h(\mathbf{x}, t) \leq \boldsymbol{\tau}_h^U \quad (8)$$
$$\boldsymbol{\tau}_r^L \leq \boldsymbol{\tau}_r(\mathbf{x}, t) \leq \boldsymbol{\tau}_r^U$$

where $\boldsymbol{\tau}_h^L$ and $\boldsymbol{\tau}_h^U$ are human lower and upper joint torque limits, and $\boldsymbol{\tau}_r^L$ and $\boldsymbol{\tau}_r^U$ are robot lower and upper limits, respectively.

(c) Human feet and robot base contacting position

$$p_{h\_feet}(t) = p_{h\_feet}^s \quad (9)$$
$$p_{r\_base}(t) = p_{r\_base}^s$$

where $p_{h\_feet}^s$ and $p_{r\_base}^s$ are the specified feet and robot base contact position on the level ground.

(d) Box forward position

$$Z_{h\_wrist}(t) - Z_{h\_pelvis}(t) \geq 0 \quad (10)$$

where Z_{h_wrist} and Z_{h_pelvis} are the global Z coordinates of wrist and pelvis points of human.

(e) Box range of motion

$$\mathbf{q}_b^L \leq \mathbf{q}_b(t) \leq \mathbf{q}_b^U \quad (11)$$

where $\mathbf{q}_b^L$ is the lower box joint angle limits and $\mathbf{q}_b^U$ is the upper limits.

(f) Box grasping location

$$p_{h_{wrist}}(t) - p_b^L(t) = 0 \quad (12)$$
$$p_{r_{end\_effector}}(t) - p_b^R(t) = 0$$

where $p_{h_{wrist}}$ and $p_{r_{end\_effector}}$ are the wrist and end-effector (EE) positions of human and robot arm, respectively. p_b^L and p_b^R are the left and right edge positions of the box.

(g) Box global EOM

$$\left|\tau_i^b\right| \leq \varepsilon, \qquad i = 1,2,3,4,5,6 \tag{13}$$

where $\boldsymbol{\tau}_b$ is the global joint force and torque values of the box, $\varepsilon = 1$ N.

(h) Exoskeleton torque limits

$$\boldsymbol{\tau}_e^L \leq \boldsymbol{\tau}_e(\mathbf{x}, t) \leq \boldsymbol{\tau}_e^U \tag{14}$$

where $\boldsymbol{\tau}_e^L$ is lower torque limit, and $\boldsymbol{\tau}_e^U$ is the upper limit for the exoskeleton.

(i) Initial and final box (hand) positions

$$p_{h\_hand}(t) = p_{h\_hand}^S(t); \qquad t = 0, T \tag{15}$$
$$p_{r\_EE}(t) = p_{r\_EE}^S(t)$$

where, $p_{h\_hand}^S$ and $p_{r\_EE}^S$ are the specified hand and end-effector (EE) positions at initial and final times.

(j) Initial and final static conditions

$$\ddot{\mathbf{q}}_h(t) = \mathbf{0}; \qquad t = 0, T \tag{16}$$
$$\ddot{\mathbf{q}}_r(t) = \mathbf{0}$$
$$\ddot{\mathbf{q}}_b(t) = \mathbf{0}$$

where $\ddot{\mathbf{q}}$ is the joint acceleration. Detailed formulations of all other constraints are referred to Arefeen & Xiang (2020, 2021), Xiang & Arefeen (2020), and Xiang et al. (2009).

Results

The nonlinear optimization problem of collaborative lifting was solved using an SQP algorithm in SNOPT. $\mathbf{P} = [\mathbf{P}_{human}, \mathbf{P}_{robot}, \mathbf{P}_{current}, \mathbf{P}_{box}] = \mathbf{0}$, $\mathbf{f}_{c1} = \mathbf{f}_{c2} = 10$ were used as the initial guesses for the optimization. The current initial guesses generate the minimal optimal objective function value after evaluating various initial guesses for the gradient-based optimization. There was a total of 229 design variables and 907 nonlinear constraints. Here, a 70W brushless DC motor (EC 45-Flat, Maxon Motors) with a gearbox ratio of 1: 79.45 was used to provide a maximum of 10 Nm output torque of the exoskeleton (Nguyen et al., 2020). The optimal solution was obtained in 136.11 seconds on a laptop with an Intel® Core™ i7 2.11 GHz CPU and 16 GB RAM. The input data related to the collaborative box-lifting task are also given in Table 1. The optimal human-robot collaborative lifting motion was presented in Figure 2. Grasping forces and exoskeleton torque were presented in Figures 3 and 4, respectively.

Table 1. Task parameters for the collaborative box lifting

Parameters	
Box weight (kg)	10
Box width (m)	0.30
Box height (m)	0.1
Box depth (m)	0.35
Initial and final human feet contact position (m)	0.375
Initial hand and end-effector position (m)	0.1
Initial and final robot base contact position (m)	0.675
Vertical final hand and end-effoctor position (m)	0.6
Horizontal final hand and end-effector position (m)	0.3
Standing distance, L (m)	1.3
T (s)	0.5

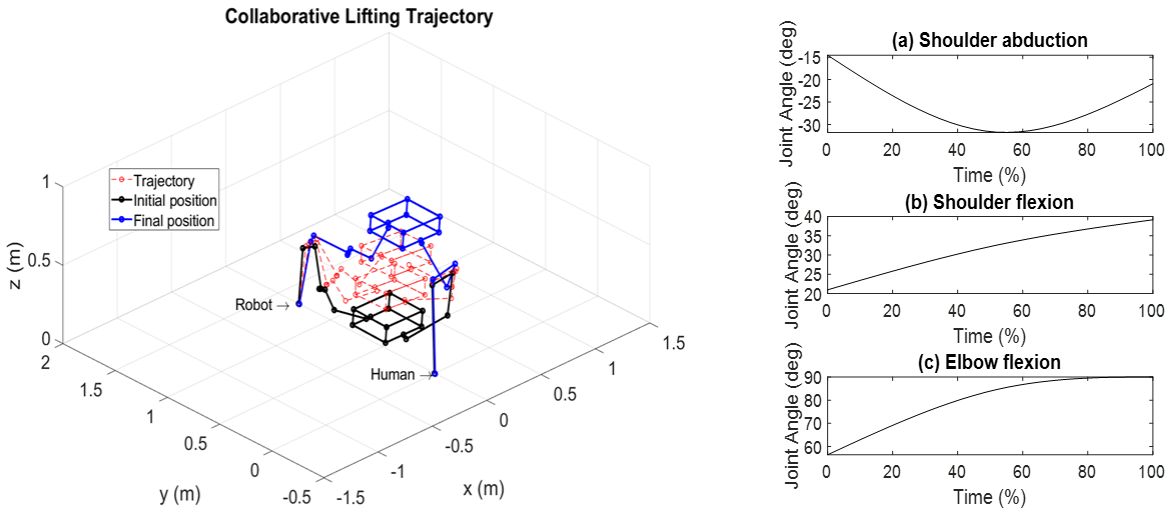

(a) (b)

Figure 2. (a) Snapshot of the human-robot arm collaborative lifting motion for a 10 kg box and (b) Human arm joint angle profiles

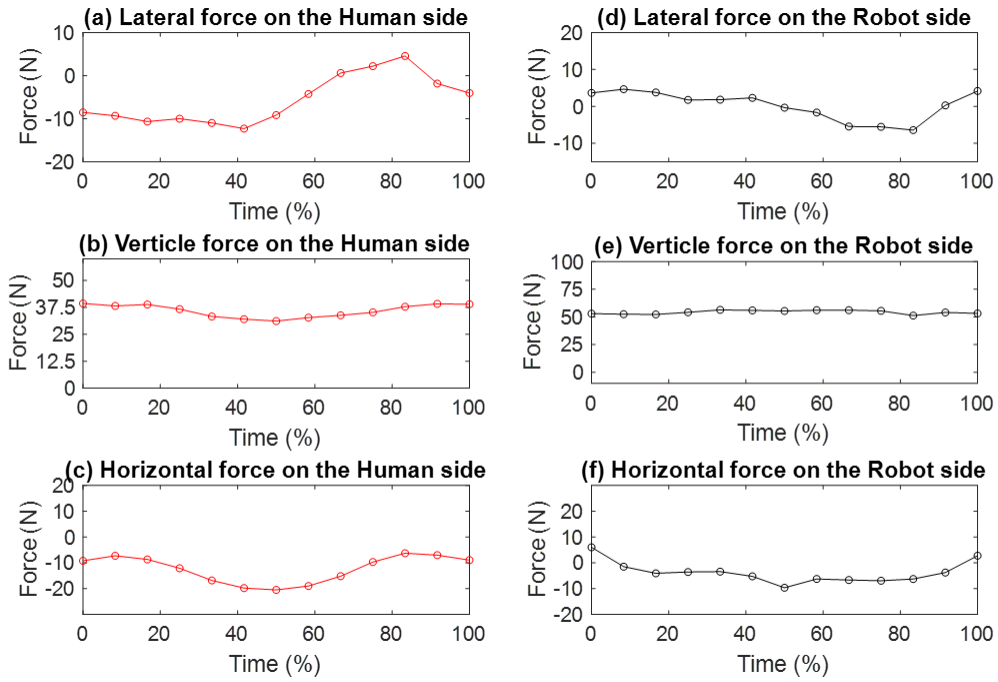

Figure 3. Box grasping forces for human-robot lifting

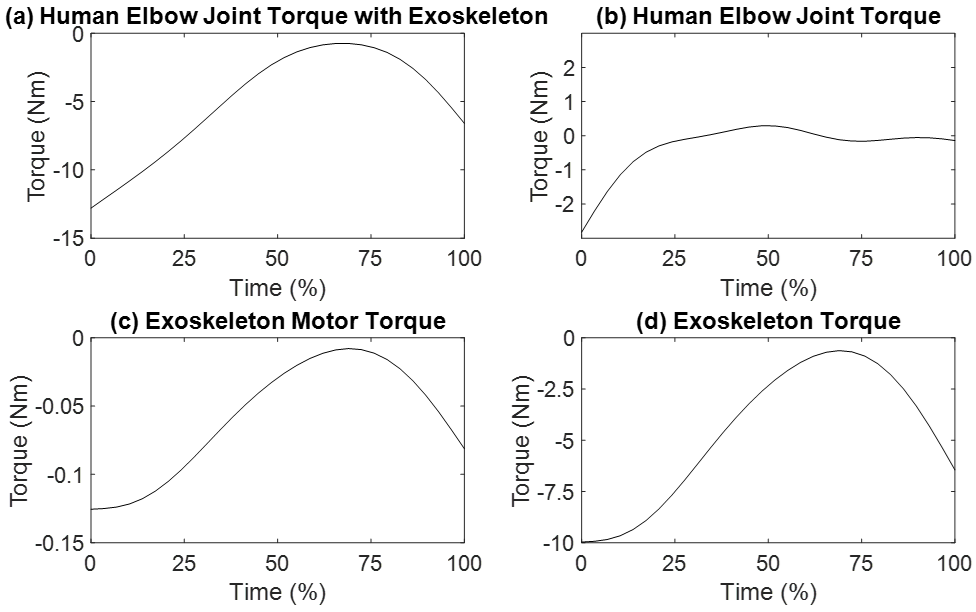

Figure 4. (a) Human elbow joint torque with an exoskeleton, (b) human elbow joint torque, (c) exoskeleton motor torque, and (d) exoskeleton output torque with a gearbox.

Discussion and Conclusions

The simulated human-robot arm lifting motion trajectory is depicted in Figure 2 (a). It is seen that the initial and final box locations are not symmetric because of the given final box location. The proposed optimization can predict a natural collaborative lifting motion. The joint angle profiles of the human arm's shoulder and elbow flexion have similar trends in the positive direction, as shown in Figure 2 (b). To maintain the box balanced, lateral and horizontal grasping forces are equal in magnitude but opposed in direction, as shown in Figure 3. In addition, the weight of the box is about equal to the total of the vertical grasping forces.

In this study, we optimized the output torque of the powered exoskeleton at the human elbow joint. The comparison of human elbow joint torque with exoskeleton assistance, human elbow torque without exoskeleton assistance, exoskeleton motor torque, and exoskeleton output torque is shown in Figure 4. It is noted that initially, the exoskeleton has maximum output torque in a negative direction. Both magnitudes of exoskeleton torque and human elbow joint torque during the lifting have decreased and then increased negatively. The exoskeleton aids the human elbow joint during the collaborative lifting process. As a result, these optimal results help to prevent human elbow joint injuries and mitigate joint fatigue during collaborative lifting.

Finally, this paper presents an optimization-based dynamic collaborative lifting motion prediction of a 13-DOF 3D human arm model with a 1-DOF exoskeleton and a 10-DOF 3D robotic arm. The simulation findings are reasonable. The collaborative lifting problem was formulated as an NLP optimization problem and efficiently solved using a gradient-based optimizer SNOPT. The results show that the proposed optimization formulation can achieve the exoskeleton's optimal control and lifting motion for the human-robot collaborative lifting task. In the future, we will validate the simulation results and apply the powered exoskeletons at multiple human joints for a lifting task.

Acknowledgments

This research was partially supported by NSF projects (CBET 1849279 and 2014281).

References

Agarwal, P., Kuo, P.H., Neptune, R. R., & Deshpande, A. D. (2013). A novel framework for virtual prototyping of rehabilitation exoskeletons. In *2013 IEEE 13th International Conference on Rehabilitation Robotics (ICORR)* (pp. 1-6), Seattle, WA, USA. 24-26 June 2013.

Arefeen, A., Quarnstrom, J., Syed, S. P. Q., Bai, H., & Xiang, Y. (2022a). Human-robot collaborative lifting motion prediction and experimental validation. *International Journal of Intelligent Robotics and Applications.* (under review).

Arefeen, A., Quarnstrom, J., Syed, S. P. Q., Bai, H., & Xiang, Y. (2022b). Human grasping force prediction, measurement, and validation for human-robot lifting. In *2022 International Design Engineering Technical Conferences and Computers and Information in Engineering Conference*, St. Louis, Missouri, August 14 – 17, 2022. (accepted).

Arefeen, A., & Xiang, Y. (2020). Two-dimensional team lifting prediction with different box weights. *Proceedings of the ASME 2020 International Design Engineering Technical Conferences and Computers and Information in Engineering Conference. Volume 9: 40th Computers and Information in Engineering Conference (CIE).* Virtual, Online. August 17–19, 2020. V009T09A004. ASME.

Arefeen, A., & Xiang, Y. (2021). Design human-robot collaborative lifting task using optimization. *Proceedings of the ASME 2021 International Design Engineering Technical Conferences and Computers and Information in Engineering Conference. Volume 2: 41st Computers and Information in Engineering Conference (CIE).* Virtual, Online. August 17–19, 2021. V002T02A010. ASME.

Bai, S., & Rasmussen, J. (2011). Modelling of physical human-robot interaction for exoskeleton designs. The Proceedings of Multibody Dynamics 2011, ECCOMAS Thematic Conference.

Cheng, H., Obergefell, L., & Rizer, A. (1994). Generator of body (GEBOD) manual. Armstrong Laboratory, Air Force Material Command.

Gill, P. E., Murray, W., & Saunders, M. A. (2005). SNOPT: An SQP algorithm for large-scale constrained optimization. *SIAM review, 47*(1), 99-131.

Manns, P., Sreenivasa, M., Millard, M., & Mombaur, K. (2017). Motion optimization and parameter identification for a human and lower back exoskeleton model. *IEEE Robotics and Automation Letters, 2*(3), 1564-1570.

Nguyen, V. Q., LaPre, A. K., Price, M. A., Umberger, B. R., & Sup IV, F. C. (2020). Inclusion of actuator dynamics in simulations of assisted human movement. *International Journal for Numerical Methods in Biomedical Engineering, 36*(5), e3334.

Wei, W., Zha, S., Xia, Y., Gu, J., & Lin, X. (2020). A hip active assisted exoskeleton that assists the semi-squat lifting. *Applied Sciences, 10*(7), 2424.

Xiang, Y., & Arefeen, A. (2020). Two-dimensional team lifting prediction with floating-base box dynamics and grasping force coupling. *Multibody System Dynamics, 50*(2), 211-231.

Xiang, Y., Arora, J. S., Rahmatalla, S., & Abdel-Malek, K. (2009). Optimization-based dynamic human walking prediction: One step formulation. *International Journal for Numerical Methods in Engineering, 79*(6), 667-695.

Zhang, T., & Huang, H. (2018). A lower-back robotic exoskeleton: Industrial handling augmentation used to provide spinal support. *IEEE Robotics & Automation Magazine, 25*(2), 95-106.

Zhou, L., Bai, S., Andersen, M. S., & Rasmussen, J. (2015). Modeling and design of a spring-loaded, cable-driven, wearable exoskeleton for the upper extremity. *Modeling, Identification and Control (Online), 36*(3), 167-177.